Rotor experiments in controlled conditions continued: New Mexico

K. Boorsma, J.G. Schepers

ECN Wind Energy, Westerduinweg 3, 1755 LE Petten, The Netherlands

E-mail: boorsma@ecn.nl

Abstract. To validate and reduce the large uncertainty associated with rotor aerodynamic and acoustic models, there is a need for detailed force, noise and surrounding flow velocity measurements on wind turbines under controlled conditions. However, high quality wind tunnel campaigns on horizontal axis wind turbine models are scarce due to the large wind tunnel size needed and consequently high associated costs. To serve this purpose an experiment using the Mexico turbine was set-up in the large low speed facility of the DNW wind tunnel. An overview of the experiments is given including a selection of results. A comparison of calculations to measurements for design conditions shows a satisfactory agreement.

In summary, after years of preparation, ECN and partners have performed very successful aerodynamic experiments in the largest wind tunnel in Europe. The comprehensive high quality database that has been obtained will be used in the international Mexnext consortium to further develop wind energy aerodynamic and acoustic modeling.

1. Introduction

Uncertainty in aerodynamic load prediction is an important parameter driving the price of wind energy [1, 2]. To reduce this uncertainty, measurements on the Mexico wind turbine were carried out in the Large Scale Low Speed Facility (LLF) of the German Dutch Wind Tunnels (DNW) [3] in 2006. One of the special features of this experiment is that in addition to the loads also flow velocities were measured using Particle Image Velocimetry (PIV). Analysis of the Mexico experiment has been performed within the framework of IEA Wind Task 29 Mexnext. The results from this project are summarized in [2]. One of the recommendations was to perform additional tests with the still available model in the DNW.

Within the EU ESWIRP project [4], budget became available to sponsor the tunnel time of a new Mexico test in the DNW. The New Mexico experiment was integrated in the EU INNWIND project as it will provide important information for the development of new high tip speed turbine concepts. Therefore a financial contribution to prepare

and supervise the experiment was granted by the EU INNWIND project. In 2014 the New Mexico experiment was carried out, illustrated in Figure 1. An overview of the experiment and its preparation is given including a selection of results together with a comparison to calculations.

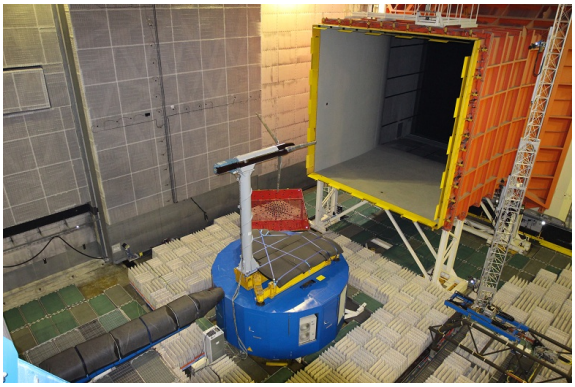

(a) Test set-up

(b) Smoke visualization

Figure 1. Illustrations of the experiment

2. Objectives

Three main objectives were identified for the experiment.

- Outstanding Mexnext research questions
  The most important question arising from Mexnext concerns the relation between measured loads and velocities. Both CFD codes as well as lifting line methods (with input of sectional aerodynamic coefficients) have overpredicted the loads compared to the measurements [2]. In addition to overprediction of the loads, the velocities are (against expectations) overpredicted as well in comparison to the experiment.
- Validate and complement first Mexico campaign
  To preserve the validity of the previous dataset and validate the settings of the new measurements, part of the previous measurements had to be reproduced. In addition to that the current database should be complimented with improved standstill, dynamic inflow (pitch steps), and inboard PIV measurements.
- Additional priorities
  In addition to the reproducing and complimenting the previous database, several new measurements were planned. These are discussed in section 4.

3. Test set-up

The set-up of the experiment was largely identical to the first Mexico campaign, featuring an open jet configuration. A difference with the previous campaign lies in the acoustic lining that was added to the tunnel floor. In addition to that, the external balance was covered with foam padding to prevent noise from the tunnel jet shear layer possibly impinging on the balance. A picture of the set-up is added in Figure 1(a).

The model features a three-bladed 4.5 m diameter upwind rotor, including a speed controller and pitch actuator. The model is instrumented with unsteady pressure sensors at five sections, distributed over the three blades. Strain gauges were added to the root of the blades to measure flap- and edgewise bending moments. Several model related sensors were installed in the nacelle (e.g. generator torque, 1p sensor, accelerometer and inclinometer) to track turbine performance. The model was suspended to a 6 component balance at the tower foot to measure forces and moments. Phase locked stereo PIV measurements were performed a the 9 o'clock plane of the rotor for a variety of configurations and locations to characterize near wake flow, rotor induction and verify the assumptions of streamtube theory. An acoustic array was positioned between nozzle exit and the model, below the jet. In addition to that, far field microphones on the side wall of the test chamber were used. More details about test set-up and instrumentation can be found in [5, 6].

4. Test matrix

Within Mexnext, the tunnel calibration from the first campaign as determined and used by the DNW has been a point of discussion. Therefore it is chosen to perform an empty tunnel calibration prior to the model test. To verify the tunnel calibration it was decided to perform a test with the model in parked conditions and a pitot tube mounted between the blades. This allowed to check the incident velocity in the rotor plane and validate the PIV system which was also used in this configuration.

Then a repeat of several pressure and PIV runs from the first Mexico campaign was performed, which together with the velocity verification provided answers towards the discrepancy of the loads-velocity relation from momentum theory. In addition to the pitch angle traverse in axial flow during standstill , the model was misaligned at various yaw angles with the blades pitched to vane. Because in misaligned flow the blades are experiencing different inflow conditions and the sectional pressure sensors are distributed between the blades, these tests were performed at 0°, 120° and 240° azimuth angles.

A full sweep through the operational regime was then performed in axial flow conditions, which included lambda traverses for both 324 rpm and 424 rpm at various pitch angles. Here the roughness strips were removed from the outboard part of the blades. An enormous amount of PIV data was acquired for this configuration (Figure 2), consisting of both axial and radial traverses at several blade azimuth angles in axial and yawed inflow conditions.

Several dynamic inflow runs were performed, consisting of rpm ramps (324 rpm to 424 rpm and back) and pitch angle steps (-2.3° to 5° and back) at various operational conditions (tip speed ratios λ=5.5, 6.7 and 10). In addition to the previous Mexico campaign the dynamic inflow runs were also performed at 15° and 30° yaw.

Pressure runs at yaw angles between -30° and 45° and various tunnel speeds (mostly at -2.3° pitch angle) were performed to study yaw effects. An 8° misalignment case was added because it is prescribed in the IEC load case calculations. Several blade add-ons were tested out on the turbine. All of them featured a full sweep through the rotating operational regime, just as was performed for the clean configuration. Also a pitch angle sweep in standstill for attached flow conditions was added to deduce the effect of the add-ons on the 'two-dimensional' polars. Firstly Guerney flaps were applied to the blade

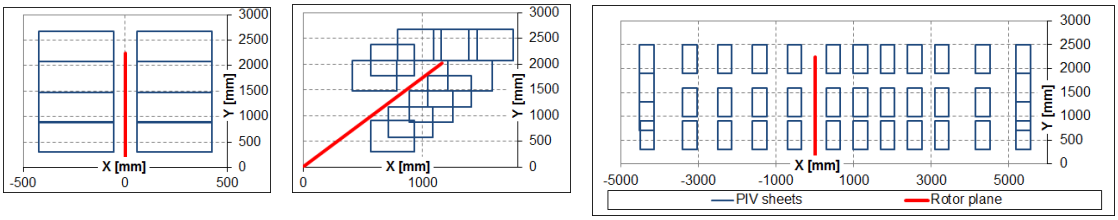

(a) Radial traverse (axial flow))

(b) Radial traverse (-30° yawed flow)

(c) Momentum traverse

Figure 2. Overview of selected PIV sheet configurations indicated by blue rectangles (coordinate system originating in rotor center: x downwind, y sideways, z upward)

up to 60%R, later they were cut off to extend to 46%R. Then 3D-printed spoilers were applied to the transition from the cylindrical part of the first streamlined section of the blades. The same manufacturing technique was used to produce serrations, which were designed to extend from roughly 70%R to 90%R. Unfortunately due to time restrictions only three 10%R wide strips were manufactured and only the 80%R to 90%R section was covered on the blades. An illustration of the add-ons is given in Figure 3.

(a) Guerney flap

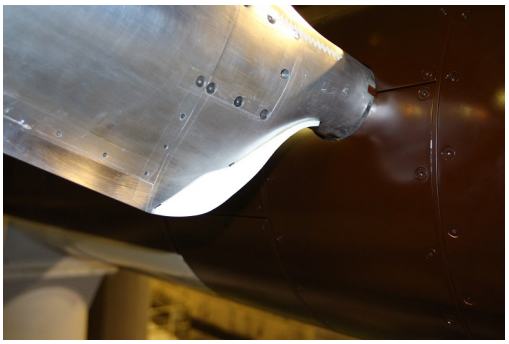

(b) Spoiler

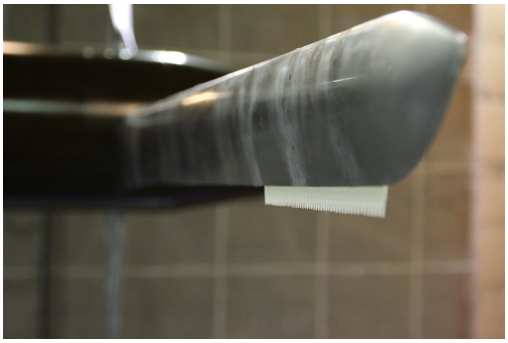

(c) Serrations

(d) Blade-off

Figure 3. Pictures of different New Mexico configurations

For the pitch misalignment runs, the pitch angle of blade 2 was reduced by 20° in comparison to the other blades. A full sweep through the operational regime was performed, featuring the standard pitch angles for blade 1 and 3. In addition to that, lambda sweeps at 15° and 20° (referring to the blade 1 and 3 pitch angle) were performed.

The flow visualization contains both oil flow visualization on the blades as well as smoke visualization by application of smoke candles from the blade tips. Blade-off measurements were performed in both rotating and standstill conditions, to provide information for determination of generator losses (with and without wind) as well as isolating rotor forces and moments.

5. Experimental results

A sample of post-processed results is given in the sections below.

5.1. Outstanding questions

To resolve the outstanding questions from the first campaign, a pressure sensors calibration and static wind tunnel test of the blades was performed at TU Delft prior to the rotating test campaign, amongst others yielding new insights with respect to calibration constants and reviving several 'dead' pressure sensors. After DNW revised the tunnel speed calibration the agreement between calculated and measured loads was greatly improved, as can be observed in Figure 7(a) for design conditions. The corresponding axial velocity traverses also reveal a much better better agreement with PIV data (see Figure 7(b)) and the the measured loads are now consistent with measured velocities, as expected from momentum theory.

5.2. Influence of roughness

The influence of roughness was assessed by removing the zig zag strip from the outboard part (last 30%R) of the blades. Figure 4 illustrates the effect on turbine performance. The pressures show an increase in lift both from the pressure and suction side of the airfoil after 30% chord. An increase in total axial force as a function of tip speed ratio of up to 5% was measured by integrating the pressures of all 5 sections over the chord and span of the blades. The corresponding power performance as a function of tip speed ratio is given in Figure 4(b). Obtaining the torque from the pressures excludes the contribution of friction and suffers from the limited resolution of pressure sensors near curved areas. This results in an overestimate of the power in comparison to obtaining this figure from the generator torque (correcting for generator losses). The fact that the generator measurements do indicate a much more significant increase in power than obtaining this figure from the pressure sensors indicates that roughness primarily influences the viscous contribution to the torque.

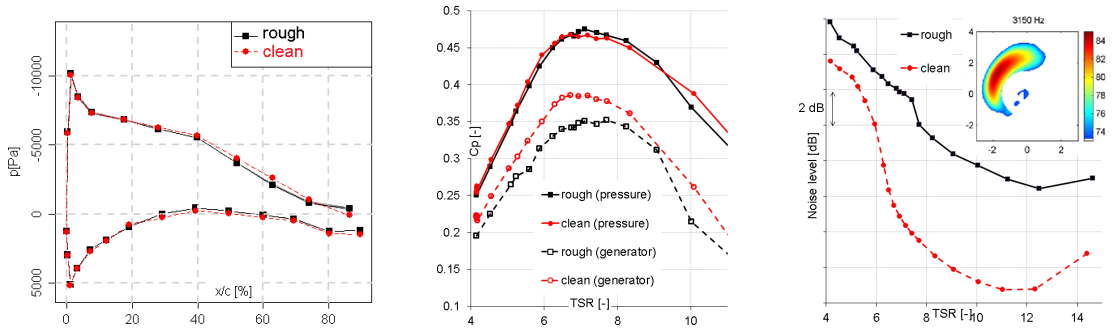

(a) Pressure distributions at 92%R, $\lambda = 6.7$ (design condition)

(b) Power coefficient Cp versus λ

(c) Noise variation with tip speed ratio (inset: beamforming plot)

Figure 4. Comparison between clean and rough configuration at 424 rpm, -2.3° pitch

The effect of roughness on the noise is illustrated in Figure 4(c). A rather large noise level decrease of 6dB maximum was measured by integrating the beamforming plots over the rotor area for all 1/3 Octave band frequencies. The difference decreases towards lower tip speed ratios because at higher angles of attack the natural transition creeps forward (coming closer to the fixed transition at the nose of the rough case) and separated flow features start to dominate the noise emission. This effect also explains why the variation of noise levels with tip speed ratio is larger for the clean configuration.

5.3. Flow field visualization

Velocity contours around the blade passage can be obtained from concatenating the PIV radial traverse sheets for several blade azimuth angles. Figure 5 shows the animation result for the three velocity components in axial, radial and tangential direction respectively. The upwash prior to and the downwash after the blade passage are visible from the axial velocity plots. The release of the tip vortex can clearly be identified from the u- and v-component, while the root vortex can also be observed in the w-component due to its different orientation. Although the release of the tip vortex is slightly inboard from the tip location at y=2.25m, tracking of the tip vortex displacement in radial direction confirms the wake expansion directly after the release, most dominant for the high tip speed ratio case. This seems to be in contradiction with previous work [7], which suggested an inboard motion of the tip vortex for the first azimuth angles after release.

The viscous blade wake can be seen to propagate downstream from the w-component. The high tip speed ratio case features a turbulent wake state and the convection speed of the blade wake varies significantly as a function of blade radius. For the low tip speed ratios the blade features high local angles of attack and hence separated flow results in a thick wake deficit contrary to the other two tip speed ratios. Because the separated flow areas are more susceptible for the centrifugal force acting on it (driving 3d rotational effects), the blade wake can also be noted in the radial velocity component for this operational condition.

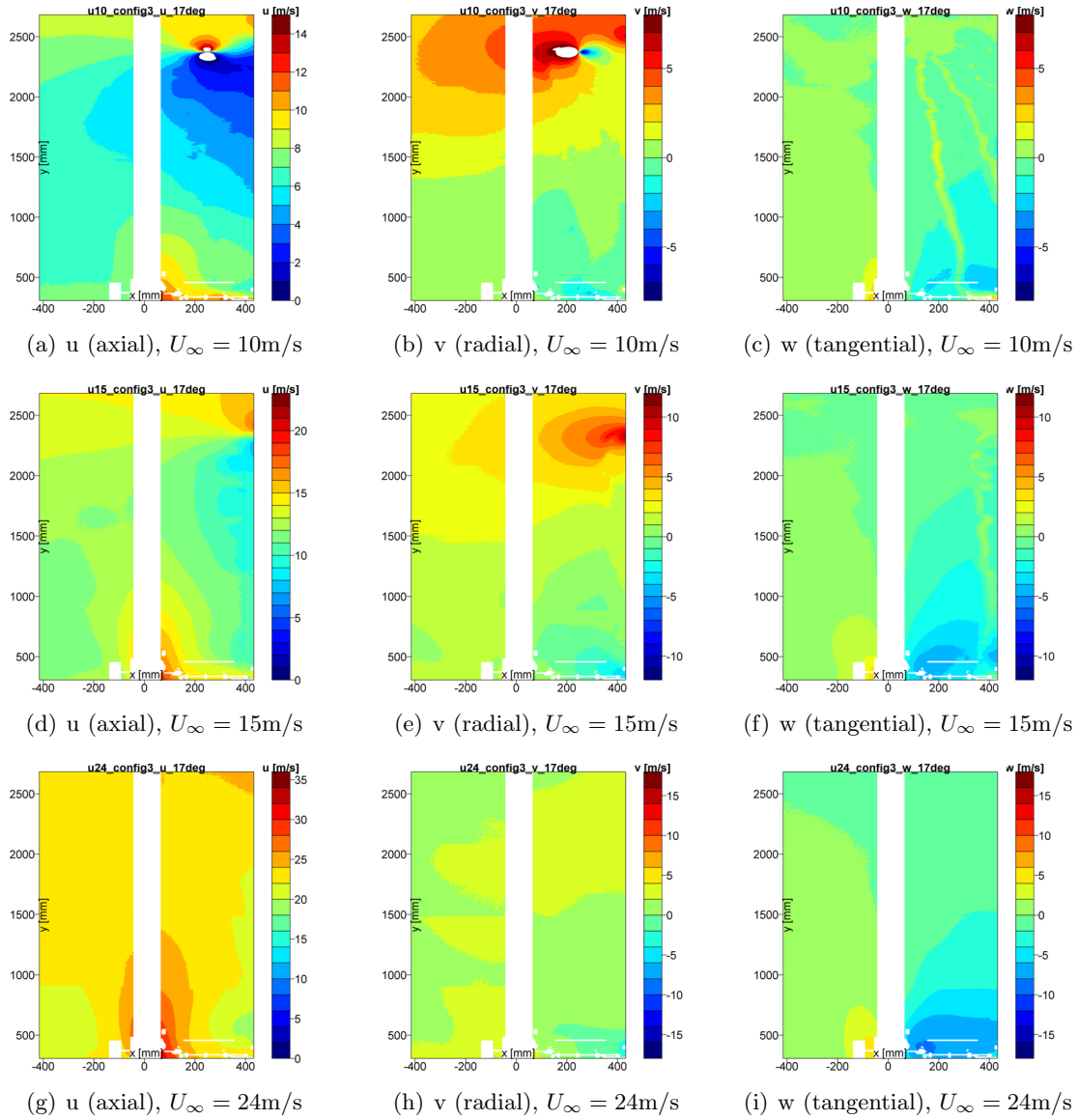

(a) u (axial), $U_\infty = 10$m/s (b) v (radial), $U_\infty = 10$m/s (c) w (tangential), $U_\infty = 10$m/s

(d) u (axial), $U_\infty = 15$m/s (e) v (radial), $U_\infty = 15$m/s (f) w (tangential), $U_\infty = 15$m/s

(g) u (axial), $U_\infty = 24$m/s (h) v (radial), $U_\infty = 24$m/s (i) w (tangential), $U_\infty = 24$m/s

Figure 5. Animation of velocity contour variation with azimuth around the blade passage (30° azimuth) for $\lambda = 10$ (top), $\lambda = 6.7$ (middle),$\lambda = 4.2$ (bottom), -2.3° pitch

5.4. Add-ons

Guerney flaps were applied in two different configurations, namely up to 60%R and 46%R, and are assessed using the pressure sensors and generator torque in Figure 6. The pressure distribution at 35%R shows the increased camber induced by the flap creates more lift both on pressure and suction side of the airfoils. The spanwise extent of the different Guerney flap configurations can be observed from the radial distribution of chord normal force. The power values obtained from the generator torque reveals that the

extra lift from the long Guerney flaps adds more power for low tip speed ratios, but this is outbalanced by the extra drag for the higher tip speed ratios. As such the occurrence of maximum Cp shifts to a lower tip speed ratio in comparison to the reference. Since the drag penalty influences rotor performance to a lesser extent for the inboard sections, the shorter Guerney flap seems to have the best of both worlds resulting in a power increase for all measured tip speed ratios. This is a promising result, although the corresponding axial force also increases significantly and the question remains whether this power increase can also be obtained with a different inboard planform design.

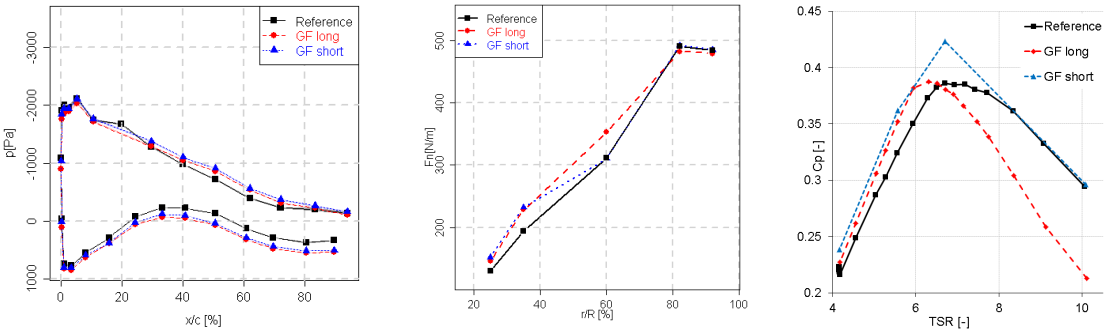

(a) Pressure distributions at 35%R, $\lambda = 6.7$ (design condition)

(b) Radial distribution of chord normal force, $\lambda = 6.7$ (design condition)

(c) Power coefficient Cp (from generator) versus λ

Figure 6. Application of Guerney flaps at 424 rpm, -2.3° pitch

6. Comparison to calculations

A comparison to lifting line calculations was performed, where both BEM as well as vortex wake (AWSM) simulations were carried out using the `ECN Aero-Module` [8]. In addition to the BEM and AWSM free wake results, also AWSM simulations were ran using a prescribed wake formulation. A hybrid free-prescribed wake was adopted, drastically reducing the computational effort. Here only a small portion of the near wake was free, whilst the convection of the remainder was prescribed based on the calculated blade induction. Figure 7 shows a selection of the results.

The calculated normal force in Figure 7(a) generally agrees well with the experiment. The measured loads are obtained from the pressure sensors while the lifting line method uses prescribed airfoil data originating from dedicated two dimensional tests. An exception to the good agreement lies in the midboard section. This could well be explained by excessive tripping of the boundary layer and is under investigation within the framework of IEA Task 29 Mexnext.

The vortex wake method allows for computing induced velocities in the external field and hence a comparison can be made to PIV measurements. The axial traverse of the axial velocity in Figure 7(b) shows an excellent agreement for the blockage upwind and a small under prediction of the velocity in the wake. The influence of using the prescribed wake starts to become visible after a meter downstream, although this is too far aft to

influence the loads. An azimuth average was made of the velocities just downstream of the rotorplane at x=0.3m and compared to the simulations in Figure 7(c) and 7(d) for axial and tangential velocity respectively. Tip and root vortex location seem to be well predicted and the calculated levels both for the axial and tangential velocities are in good agreement. The prescribed wake is shown to influence the induced velocity variation at the tip, probably because the free movement of the tip vortex slightly differs from the prescription. As mentioned in section 5.1 the measured loads are now consistent with measured velocities, as expected from momentum theory. A more in depth comparison between experiment and simulations (including CFD) featuring contributions from all over the globe is in the making within Mexnext.

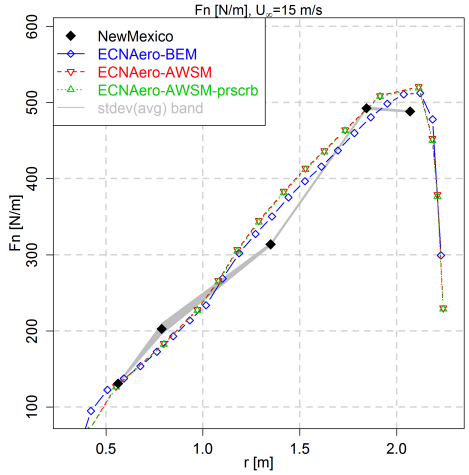

(a) Sectional normal force

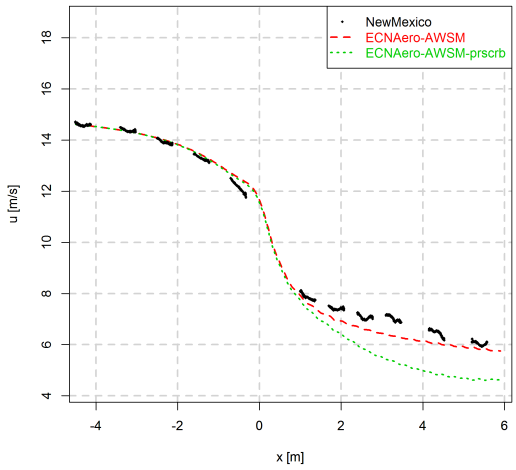

(b) Axial traverse of u, r=1.5 m, 0° azimuth

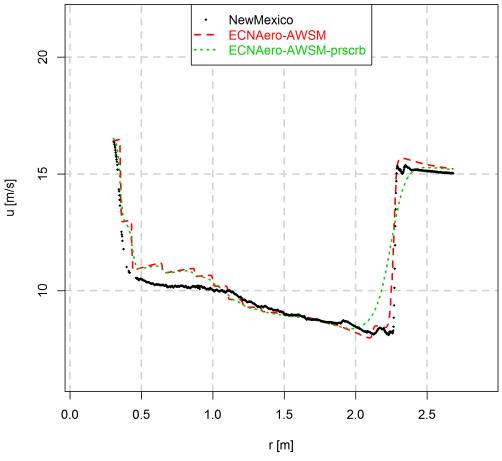

(c) Radial traverse of u, x=0.3 m, azimuth averaged

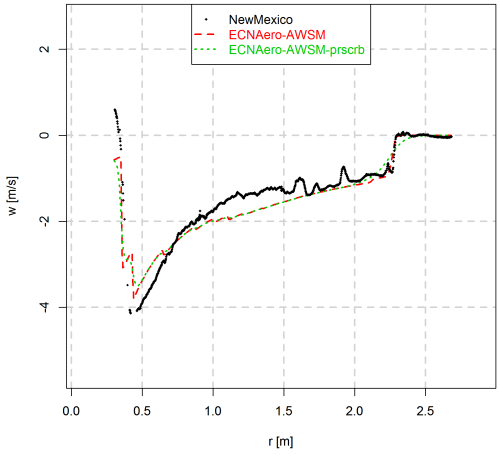

(d) Radial traverse of w, x=0.3 m, azimuth averaged

Figure 7. Comparison between measurements and simulations for design conditions at U_∞=15m/s, 424 rpm, -2.3° pitch

7. Conclusions

Several open questions from the first campaign have been resolved and a good agreement has been found between between Mexico and New Mexico measurements. The Mexico database has been extended with extra test cases to progress modeling of dynamic inflow, non-uniformity between the blades, yawed flow effects, parked conditions and pitch misalignment. In addition to that several blade add-ons were tested to improve the turbine performance. Acoustic measurements have been performed using both far field microphones as well as a microphone array. Flow visualization was performed by application of smoke candles to the blade tips and oil to the blade surface.

In summary, ECN and partners have performed very successful aerodynamic experiments in the largest wind tunnel in Europe. A comprehensive high quality database has been obtained which is shared in the wind energy R&D community. A sample of results has been shown in the current paper, however a large portion of the measurement data is still untouched. The database will be analyzed further in an international context in order to validate aerodynamic models and to advance the aerodynamic modeling of wind turbines. With the results future large wind turbines will be designed with calculation models having higher accuracy and less uncertainty.

Acknowledgements

Financial support for this work was given in part by the EU INNWIND project. In addition to that the European ESWIRP project has been responsible for sponsoring the tunnel time in the DNW. The support of the the steering committee (Delft University of Technology, Technion Israel Institute of Technology and DTU Technical University of Denmark), which advised during the preparation of the tunnel test, was greatly appreciated. Shafiek Ramdin is acknowledged for providing part of the simulation results.

References

[1] J.G. Schepers and K. Boorsma et al. Final report of IEA Task 29, Mexnext (Phase 2). ECN-E-14-060, Energy Research Center of the Netherlands, December 2014.

[2] J.G. Schepers and K. Boorsma et al. Final report of IEA Task 29, Mexnext (Phase 1): Analysis of MEXICO wind tunnel measurements. ECN-E-12-004, Energy Research Center of the Netherlands, February 2012.

[3] J.G. Schepers and H. Snel. MEXICO, Model experiments in controlled conditions. ECN-E-07-042, Energy Research Center of the Netherlands, 2007.

[4] http://www.eswirp.eu/. In *European Strategic Wind tunnels Improved Research Potential*, 2014.

[5] K. Boorsma and J.G. Schepers. Description of Experimental Setup, New Mexico Experiment. Technical Report ECN-X–15-093, ECN, August 2015.

[6] K. Boorsma and J.G. Schepers. New MEXICO Experiment, Preliminary overview with initial validation. Technical Report ECN-E–14-048, ECN, September 2014.

[7] G.A.M. van Kuik, D. Micallef et al. The role of conservative forces in rotor aerodynamics . *Journal of Fluid Mechanics*, 750, 2014.

[8] K. Boorsma, F. Grasso, and J.G. Holierhoek. Enhanced approach for simulation of rotor aerodynamic loads. Technical Report ECN-M–12-003, ECN, presented at EWEA Offshore 2011, Amsterdam, 29 November 2011 - 1 December 2011, 2011.